The Impact of Tropical Pacific SST Biases on the S2S Forecast Skill over North America in the UFS Global Coupled Model

CRISTIANA STAN,[a] V. KRISHNAMURTHY,[a] HEDANQIU BAI,[a] BIN LI,[b] AVICHAL MEHRA,[c] JESSICA MEIXNER,[c] SHRINIVAS MOORTHI,[c] LYDIA STEFANOVA,[b] JIANDE WANG,[b] JUN WANG,[c] DENISE WORTHEN,[b] AND FANGLIN YANG[c]

[a] *Department of Atmospheric, Oceanic and Earth Sciences, George Mason University, Fairfax, Virginia*
[b] *IMSG, NOAA/NCEP/EMC, College Park, Maryland*
[c] *NOAA/NCEP/EMC, College Park, Maryland*

(Manuscript received 27 March 2022, in final form 2 November 2022)

ABSTRACT: The impact of tropical Pacific sea surface temperature (SST) biases on the deterministic skill of the Unified Forecast System (UFS) coupled model Prototype 5 is evaluated during weeks 1–4 of the forecast. The evaluation is limited to the contiguous United States (CONUS) and two seasons: boreal summer (June–September) and winter (December–March). The tropical SST in the UFS model is warmer than in observations and bias patterns show seasonal dependence especially in the central and western Pacific. During boreal summer, the bias is located north of the equator whereas in winter, the bias is located in the Southern Hemisphere. A regression analysis indicates a significant relationship between these SST biases and the biases in the surface temperature and precipitation over the CONUS along with midtroposphere large-scale circulation and North Pacific storm-track activity. The SST biases affect the biases in other fields from week 1 of the forecast and the impact becomes stronger as the lead time increases to week 4. The impact of SST biases on the biases in other fields show a qualitative relationship to the patterns of forecast errors of the fields.

KEYWORDS: Hindcasts; Operational forecasting; Model errors; Model evaluation/performance; Numerical weather prediction/forecasting

1. Introduction

Teleconnections of tropical sea surface temperature (SST) modes represent one of the sources of predictability on subseasonal-to-seasonal time scales (S2S) for the surface weather over the contiguous United States (CONUS; Johnson et al. 2014; Krishnamurthy et al. 2021). Thus, systematic errors, also known as biases, in the SST prediction can affect the forecast skill of S2S forecast systems. Biases in the SST are common problems in ocean–atmosphere coupled models and the sources of these systematic errors are associated with many reasons including, but not limited to, horizontal resolution in the ocean (Balaguru et al. 2021), ocean–atmosphere feedbacks (Li and Xie 2014), representation of low-level clouds (Stan et al. 2010; Hu et al. 2011), and shortwave fluxes (Zuidema et al. 2016). Similar to the seasonal time scale, at S2S time scale, uncertainties in the SST initial states (Stan and Kirtman 2008) can introduce SST drifts that manifest as biases for the length of the forecast.

The usage of atmospheric models coupled to an active ocean model and sea ice model for S2S prediction has become the standard model configuration adopted by major forecasting centers only in the last few years. For example, in 2017 out of 11 operational S2S forecast systems participating in the S2S Prediction Project database, 6 used a combination of persistence of initial conditions and climatology to define the oceanic and sea ice boundary conditions (Vitart et al. 2017). As a result, the impact of SST biases on the S2S forecast skill is not well understood. Climate modeling studies offer some insight on the potential effects of SST biases through their impact on the large-scale circulation and associated moisture transports. For instance, in a recent study Johnson et al. (2020) have shown that correction of tropical SST biases in intervention experiments yields to improvements of precipitation statistics over North America. In particular, their results show that in boreal winter, negative SST biases in the extratropical North Pacific strengthen the storm track and displace it southward from its winter climatological position. These changes in the storm track can be further associated with enhanced precipitation in the southwestern United States. In boreal summer, the effect of the cold bias is a weakening of the North Pacific storm track, which can be associated with drier conditions over northern North America.

The main objective of this study is to explore the statistical link between the SST biases over the tropical Pacific and the errors in the S2S forecast of surface weather over the CONUS. The analyzed forecasts are produced with an experimental version of the S2S application of the NCEP next-generation forecast system, the Unified Forecast System (UFS). The relationship between tropical Pacific SST biases and remote biases over CONUS is investigated using a simple linear regression between the biases, with the SST bias as the predictor variable. A qualitative analysis is further applied to explore similarities between the SST-induced biases and forecast skill measured by the root-mean-square errors. While both measures are

Supplemental information related to this paper is available at the Journals Online website: https://doi.org/10.1175/JCLI-D-22-0196.s1.

Corresponding author: Cristiana Stan, cstan@gmu.edu

DOI: 10.1175/JCLI-D-22-0196.1

intended to quantitatively evaluate the quality of forecasts, they refer to different aspects of the quality (Murphy 1993). The bias measures the correspondence between the mean forecast and mean observations by comparing their marginal distributions whereas the forecast skill measures the relative accuracy over some reference skill such as persistence or climatology (Murphy 1993).

In section 2, we describe the observations, forecast system, and analyses utilized in this paper. The main biases in the tropical SST, surface temperature, and precipitation over CONUS and large-scale atmospheric circulation are presented in section 3a. The potential impact of SST biases on the other forecast biases are discussed in section 3b. Section 3c describes the qualitative results. Section 4 offers remarks and conclusions.

2. Model, data, and methods

a. Model

The numerical model used in this study is the UFS Coupled Model Prototype 5, developed by the NCEP (Krishnamurthy et al. 2021; Krishnamurthy and Stan 2022; Stefanova et al. 2022). This configuration of the UFS model consists of an atmospheric component (FV3GFS), an oceanic component (GFDL MOM6 model; Adcroft et al. 2019), a sea ice component (Los Alamos CICE6 model) with tripolar 0.25° global grid, and a component for sea waves (WW3DG 2019). The coupling of the wave model with the other components is through the National Unified Operational Prediction Capability (NUOPC) component connector. The atmosphere, ocean, and sea ice models are coupled via the Community Mediator for the Earth Prediction Systems (CMEPS). This is the first UFS prototype using CMEPS for performing custom coupling operations. FV3GFS uses the FV3 dynamical core on the cubed-sphere grid (Putman and Lin 2007; Harris and Lin 2013) and the Common Community Physics Package (CCPP) for physics parameterizations. The atmospheric component has a horizontal resolution of ~0.25° (C384) and 64 levels in the vertical. The horizontal resolution of the ocean and sea ice models is 0.25°. The UFS coupled model was utilized to generate a set of retrospective forecasts for the period April 2011–March 2018. The reforecasts are initialized on the first and fifteenth of each month (168 reforecasts for the entire period) and are 35 days long. The atmospheric initial conditions were the Climate Forecast System Reanalysis data while the Climate Prediction Center (CPC) Hybrid Global Ocean Data Assimilation System provided the initial conditions for the ocean model. The sea ice model was initialized by the CPC ice analysis and the initial conditions for the wave model were produced using forcing generated with the Climate Forecast System version 2 (CFSv2; Saha et al. 2014). Because in this study only reforecasts will be analyzed, they will be referred to as forecasts.

b. Data

The forecasts will be compared to observations and reanalysis data, which will be referred to as observations. The daily mean observational datasets include the Optimally Interpolated SST version 2 (OISST2) dataset developed by NOAA (Reynolds et al. 2007) on a 0.25° longitude × 0.25° latitude grid, CPC unified (CPCU) gauge-based analysis of daily precipitation (P. Xie et al. 2010) on a 0.5° × 0.5° grid, CPC global temperature (provided by the NOAA/OAR/ESRL) on a 0.5° × 0.5° grid, and the European Centre for Medium-Range Weather Forecasts interim reanalysis (ERA-Interim, hereafter ERAI; Dee et al. 2011) on the T255 horizontal grid (~0.703° resolution).

c. Methods

All analyses are conducted on the 0.25° longitude × 0.25° latitude grid for the consistency of analysis in each field. The forecast data were saved every 6 h. Precipitation data represent a 6-h accumulation and the other variables are instantaneous values. The 6-hourly data are converted to daily means starting from forecast hour 6. For both the observed and model data, daily climatological mean was computed as the average of calendar day over the period of the forecasts. Daily anomalies are computed by subtracting the climatological mean from daily values. Similarly, weekly means and anomalies are computed by averaging daily means and anomalies, respectively, over the week under consideration. The analysis is conducted for two seasons: boreal summer [June–September (JJAS)] and boreal winter [December–March (DJFM)].

To investigate the North Pacific storm track two methods were adopted: (i) an Eulerian measure based on the 500-hPa geopotential height (Z500) variability and (ii) a time-varying method based on the 24-h change in the large-scale circulation measured by the Z500 daily anomalies. In the Eulerian framework, a high-pass filter (8 days) is applied to extract the synoptic signal from the Z500 daily anomalies. The filter is constructed by first applying a fourth-order low-pass Butterworth filter (Hamming 1989) and then subtracting the filtered signal from daily anomalies. In the second method, the storm-track activity at each grid point is defined as

$$\Delta Z^2(t) = [\mathrm{Z500}(t + 24) - \mathrm{Z500}(t)]^2, \tag{1}$$

where Z500 denotes daily anomalies. A version of Eq. (1) based on the sea level pressure was used by Yau and Chang (2020) to characterize the storm tracks in the Northern Hemisphere.

The mean change in the biases over CONUS in response to SST biases is measured by the lag-0 regression coefficient of weekly biases. The statistical significance of regression analysis is established using the effective number of degrees of freedom developed by Bretherton et al. (1999). The effective number of degrees of freedom at each gid point is defined as

$$d = N\,\frac{1 - r_1 r_2}{1 + r_1 r_2},$$

where N is the sample size and $\{r_i;\ i = 1,2\}$ the lag-one autocorrelation of time series of predictor and predictand, respectively. The number of degrees of freedom used for the calculation of t value is an area average.

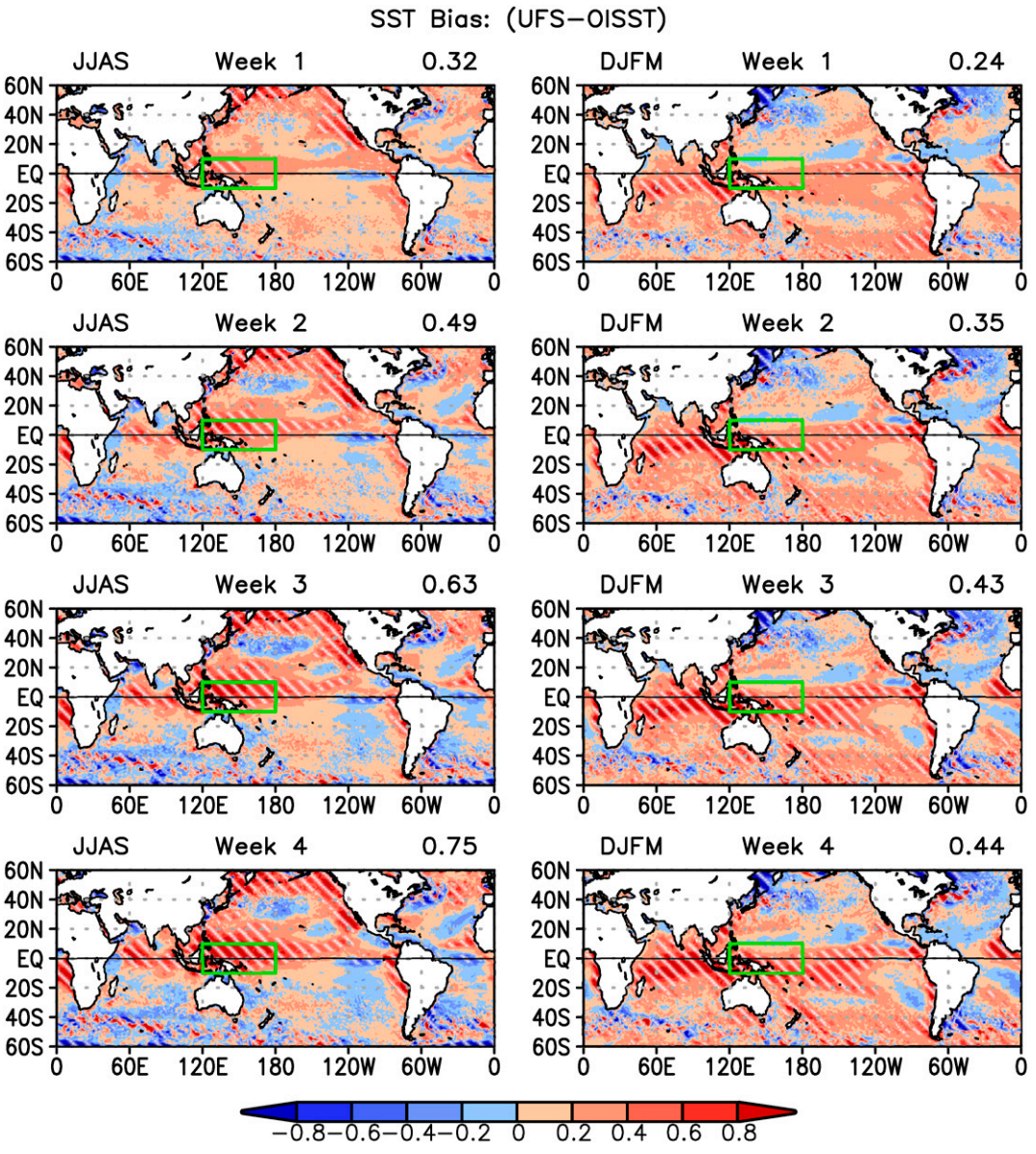

FIG. 1. Difference in the climatological mean of SST (K) between UFS forecasts and observation (OISST) for the first 4 weeks of forecasts during (left) JJAS and (right) DJFM. The forecasts initiated from the first and fifteenth each month of JJAS and DJFM during 2011–18 are used in computing the bias. The green box covering 10°S–10°N, 120°E–180° is the domain over which the equatorial SST index will be defined. Numbers in the upper-right corner represent the mean bias in the green box. Regions where the absolute value of bias is greater than 0.4° are hatched.

3. Results

a. Forecast biases

The first step in understanding the impact of SST biases is to estimate them, and Fig. 1 shows the weekly biases defined as the difference in the daily mean of SST between all UFS forecasts (both initial conditions) and observations averaged over 7 days. In both seasons, SST biases increase from week 1 through week 4. In the tropical Pacific, a positive bias appears in the hemisphere where summer is located. During boreal summer, a large positive bias develops over the warm pool region. This bias reaches maximum values (~0.6°–0.8°C) during week 3. In week 1, the warm bias (~0.4°–0.6°C) in the warm pool region is slightly higher than the bias (0.3°–0.4°C) in a prototype developed by the Met Office to become their operational coupled numerical weather prediction forecasting system (Vellinga et al. 2020). A study by Emery (2015) showed that the accuracy of buoy measured bulk SST is within ±0.4°C; therefore, only biases outside of this range represent true model errors. In Fig. 1, regions where the absolute value of the SST bias is greater than 0.4°C are highlighted. In the tropical eastern Pacific, a cold bias located at the equator in week 1

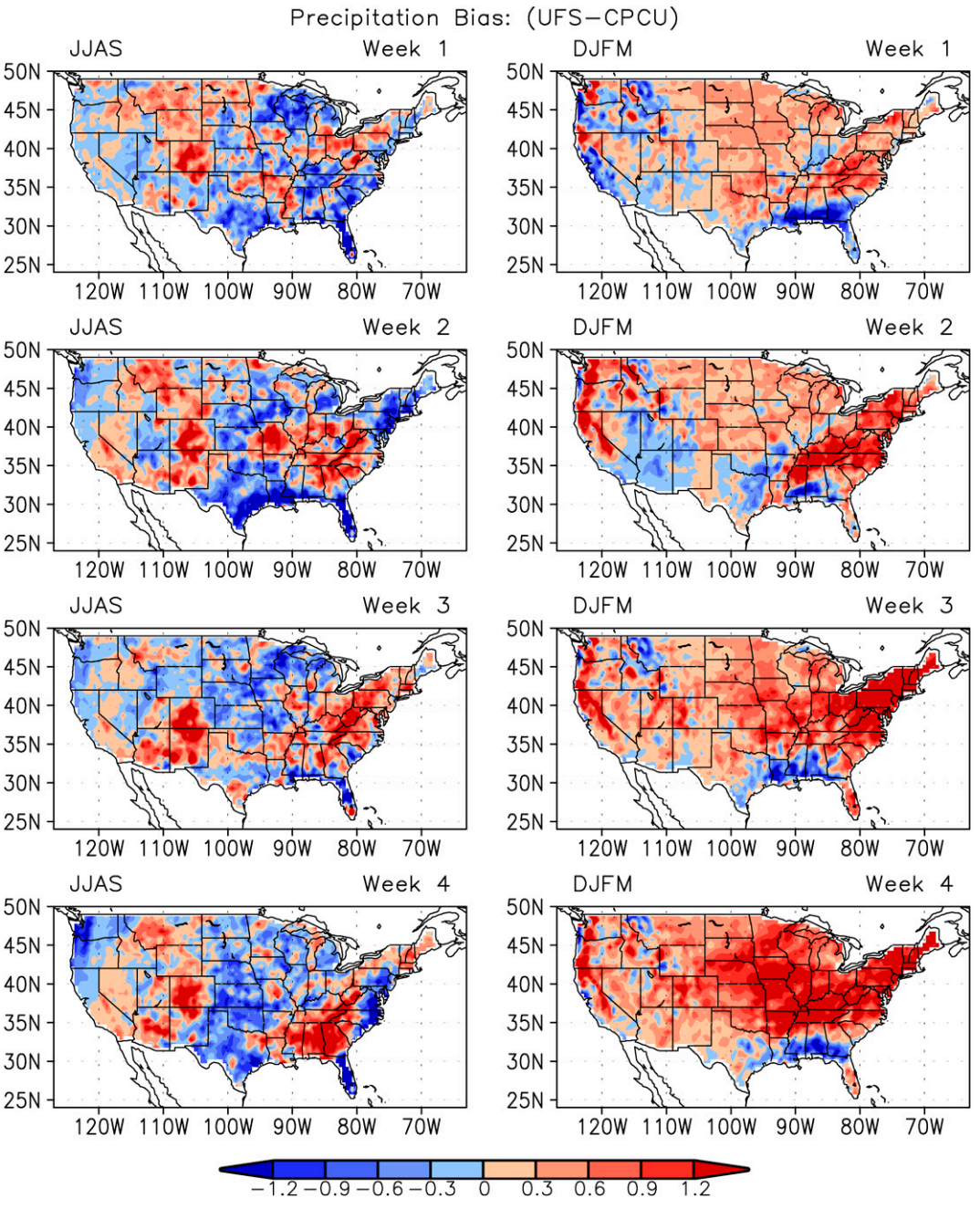

FIG. 2. Difference in the climatological mean of precipitation (mm day^{-1}) between UFS forecasts and observation (CPCU) for the first 4 weeks of forecasts during (left) JJAS and (right) DJFM. The forecasts initiated from the first and fifteenth each month of JJAS and DJFM during 2011–18 are used in computing the bias.

expands meridionally south of the equator reaching 60°S by week 4.

During boreal winter, the warm SST bias has a zonal structure across the southern tropical Pacific with a small intrusion north of the equator eastward of the date line. Just like in boreal summer, maximum SST biases during boreal winter are located over the western Pacific, but shifted over the Maritime Continent. For this reason, the region of 10°S–10°N, 120°E–180° is being used to construct an index defined as the area average of SST bias and interpreted as the SST bias in the deep tropics. In the extratropics, the forecasts develop a cold bias in the northern Pacific that amplifies and expands form week 1 through week 4 during boreal summer. In boreal winter, the extratropics are dominated mostly by weak negative SST biases in the North Pacific. Biases in other atmospheric and land parameters that can be affected by tropical

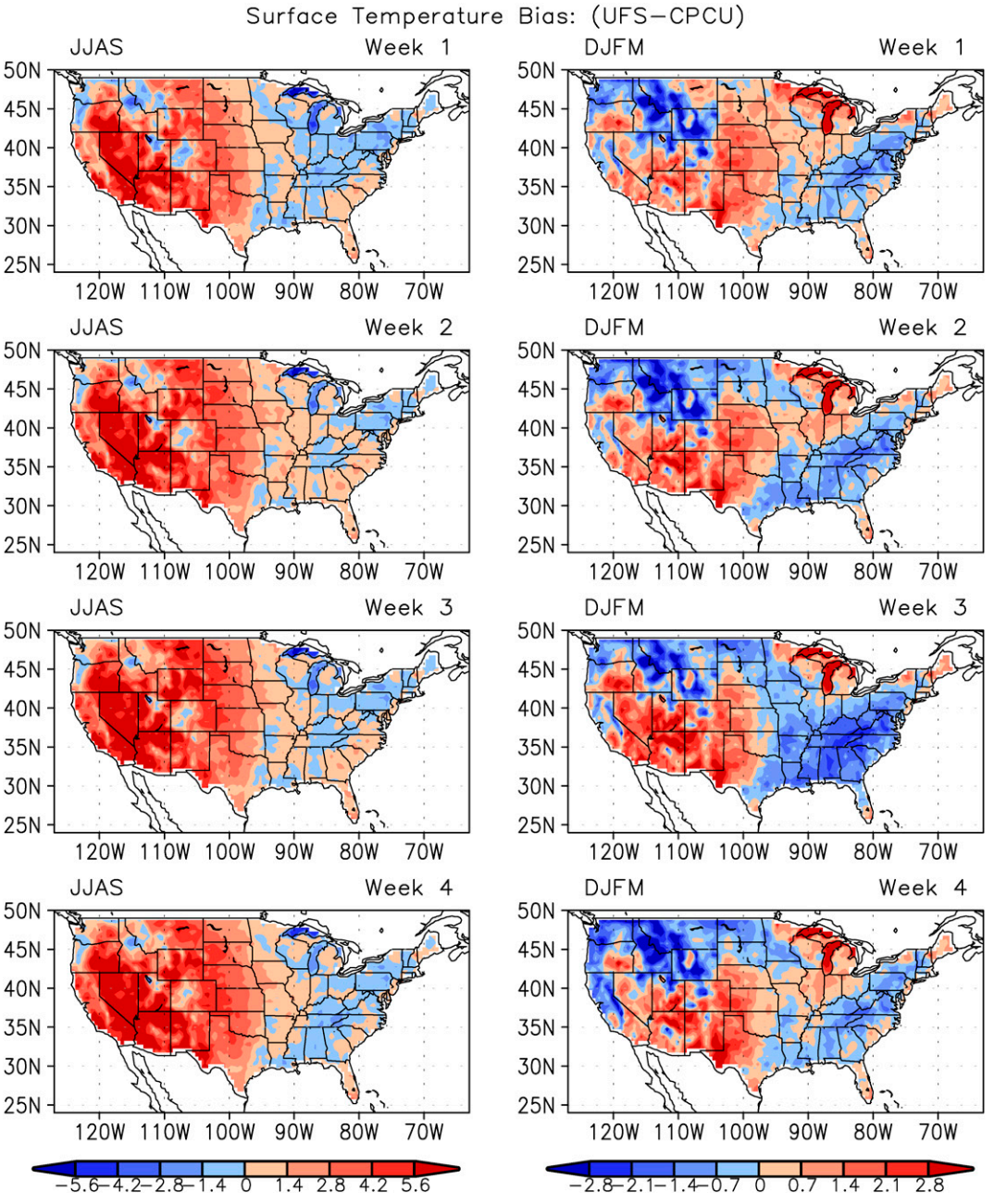

FIG. 3. Difference in the climatological mean of surface temperature (K) between UFS forecasts and observation (CPCU) for the first 4 weeks of forecasts during (left) JJAS and (right) DJFM. The forecasts initiated from the first and fifteenth each month of JJAS and DJFM during 2011–18 are used in computing the bias.

SST are shown in Figs. 2–5 for both boreal summer and winter.

During boreal winter, precipitation (Fig. 2) shows a mean wet bias (positive difference) across CONUS, with a small exception over a narrow strip along the Gulf of Mexico's northern shores. The magnitude of biases increases from about 0.3–0.4 mm day^{-1} during week 1 to about 1.2 mm day^{-1} in week 4. During boreal summer, biases are both positive and negative and show patterns that change location, shape, and sign with the forecast lead. The West Coast of the United States shows a consistent dry bias (negative difference) from week 1 through week 4 with a magnitude that increases with the forecast lead. Another region with a persistent dry bias is the peninsular Florida.

The surface temperature biases (Fig. 3) show distinct patterns for winter and summer. During boreal summer, a warm bias dominates the entire U.S. regions west of 95°W. The warm bias is almost constant over the 4 weeks of the forecast suggesting either a saturation of biases on short range time

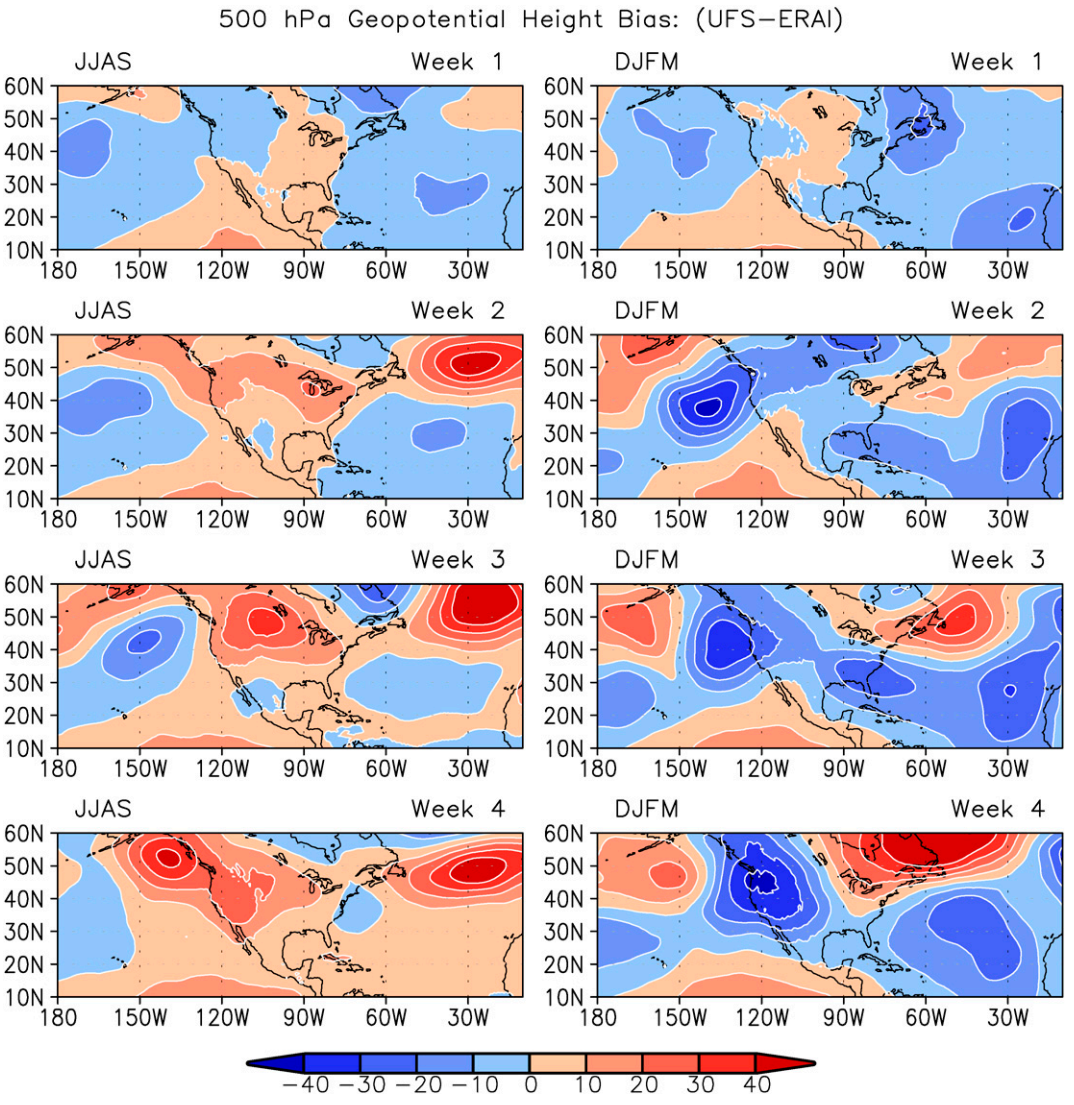

FIG. 4. Difference in the climatological mean of 500 hPa geopotential height (gpm) between UFS forecasts and reanalysis (ERAI) for the first 4 weeks of forecasts during (left) JJAS and (right) DJFM. The forecasts initiated from the first and fifteenth each month of JJAS and DJFM during 2011–18 are used in computing the bias.

scales or an influence from boundary forcing such as the SST. Biases on the other half of United States are slightly colder and with less distinct regional patterns. During boreal winter, biases are also almost constant with distinct regional patterns. A distinct diagonal strip in the southeastern United States is dominated by cold biases as well as a zonal strip above 40°N. This latitude corresponds to the rough climatological latitude of the storm track (Cook et al. 2018). Central and western U.S. regions are dominated by warm biases.

Following Johnson et al. (2020) hypothesis that changes in the storm tracks can be associated with changes in precipitation over North America, we also investigate biases in the North Pacific storm track. For this purpose, baroclinic wave activity is defined as the variance of the high-pass filtered Z500 anomalies. Figure 4 shows Z500 biases and Fig. 5 shows the difference in the variance of 8-day high-pass filtered Z500 anomalies. In both seasons, Z500 biases increase with the forecast lead. Over most of the United States, the forecasts overestimate (positive difference) the geopotential height during boreal summer and underestimate (negative difference) them during boreal winter. These regional biases are part of large-scale waves that propagate from the tropics into the extratropics. During boreal summer, a negative center that develops in the first week in the midlatitudes of the central Pacific intensifies and expands northeastward up to week 3, after which it is replaced by a positive center. Over the North Atlantic, a very small positive bias (<10 gpm), between 50° and 60°N and east of 30°W, in week 1 expends westward and intensifies to more than 40 gpm in week 4. During boreal winter, the negative center around 40°N in the eastern Pacific noticed in boreal

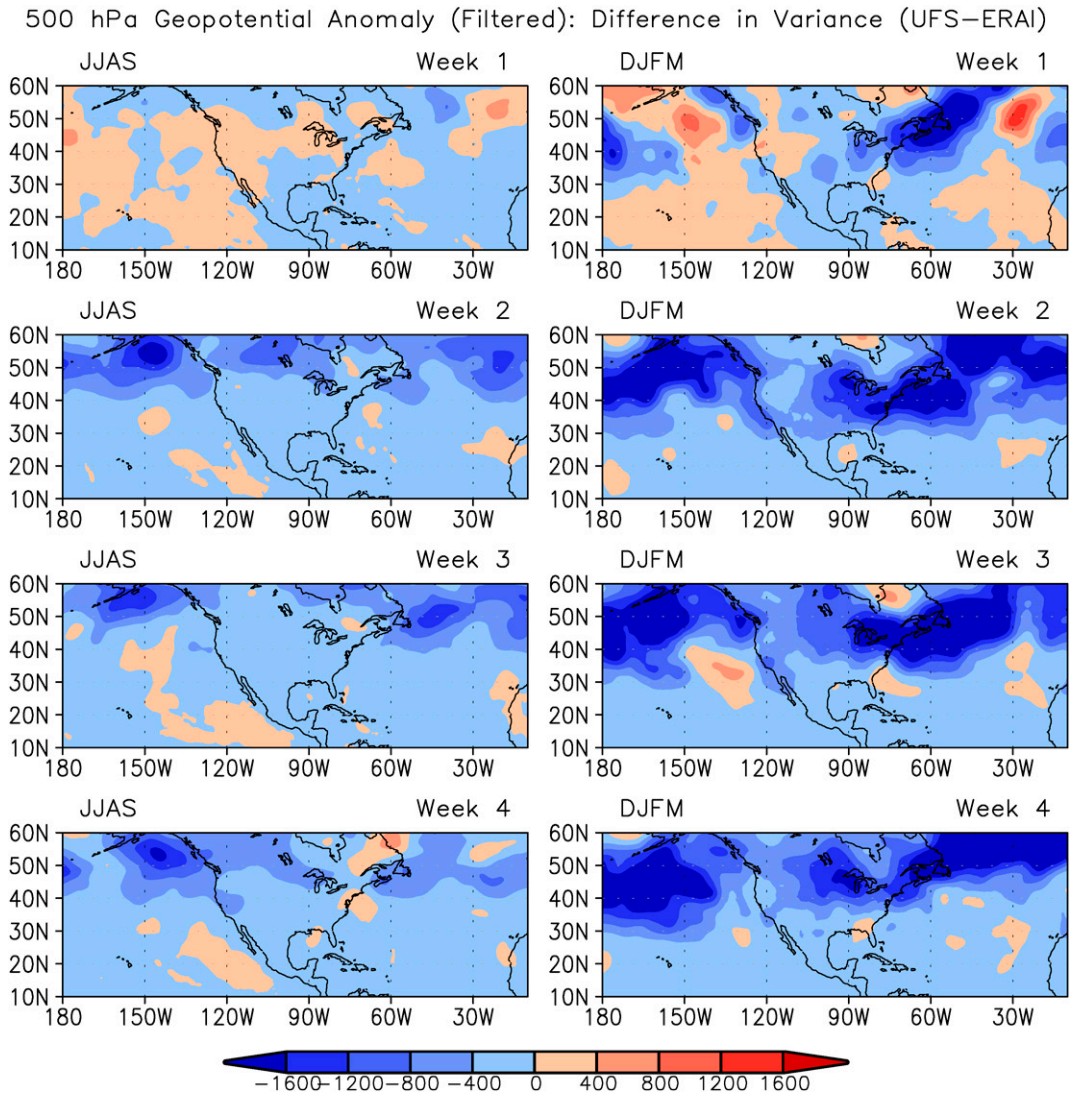

FIG. 5. Difference in the variance (gpm^2) of 8-day high-pass filtered 500 hPa geopotential height anomaly between UFS forecasts and reanalysis (ERAI) for the first 4 weeks of forecasts during (left) JJAS and (right) DJFM. The forecasts initiated from the first and fifteenth each month of JJAS and DJFM during 2011–18 are used in computing the variance.

summer persists and is flanked to the north and south by positive centers. In the Atlantic, a positive center north of 40°N and a negative center south of 40°N intensify from week 1 to week 4.

The differences between the filtered variance of the forecast and observation suggest that forecasts underestimate the strength of the storm tracks in both seasons and the errors are larger during boreal winter. The bias patterns seen in the storm-track activity measured by the Z500 filtered variance are reproduced when ΔZ^2 is used as a storm-track metric (Fig. S1 in the online supplemental material).

b. *Impacts of SST bias*

The relationship between the tropical SST biases over the western Pacific and the biases in the other fields described above are evaluated using a linear regression method. In this method, biases in the atmospheric and land parameters are regressed onto the standardized index of the equatorial SST bias (defined earlier in section 3a). A caveat of the analysis presented here is that only lag-0 regression is considered. The persistence of tropical SST bias suggests that analysis for other lags will not change the results. In Fig. 1 the mean value of the equatorial SST bias index is shown for each week. While in week 1 the mean value of the index is within the margin of measurement errors, the regression for lead 1 week is still shown for completeness of analysis. In week 2 of winter, the mean value of the SST index is also smaller than the measurement errors. If the box is shifted slightly southward the mean value of the index is larger than the threshold errors. The position of the box is kept fixed for the consistency of the analysis.

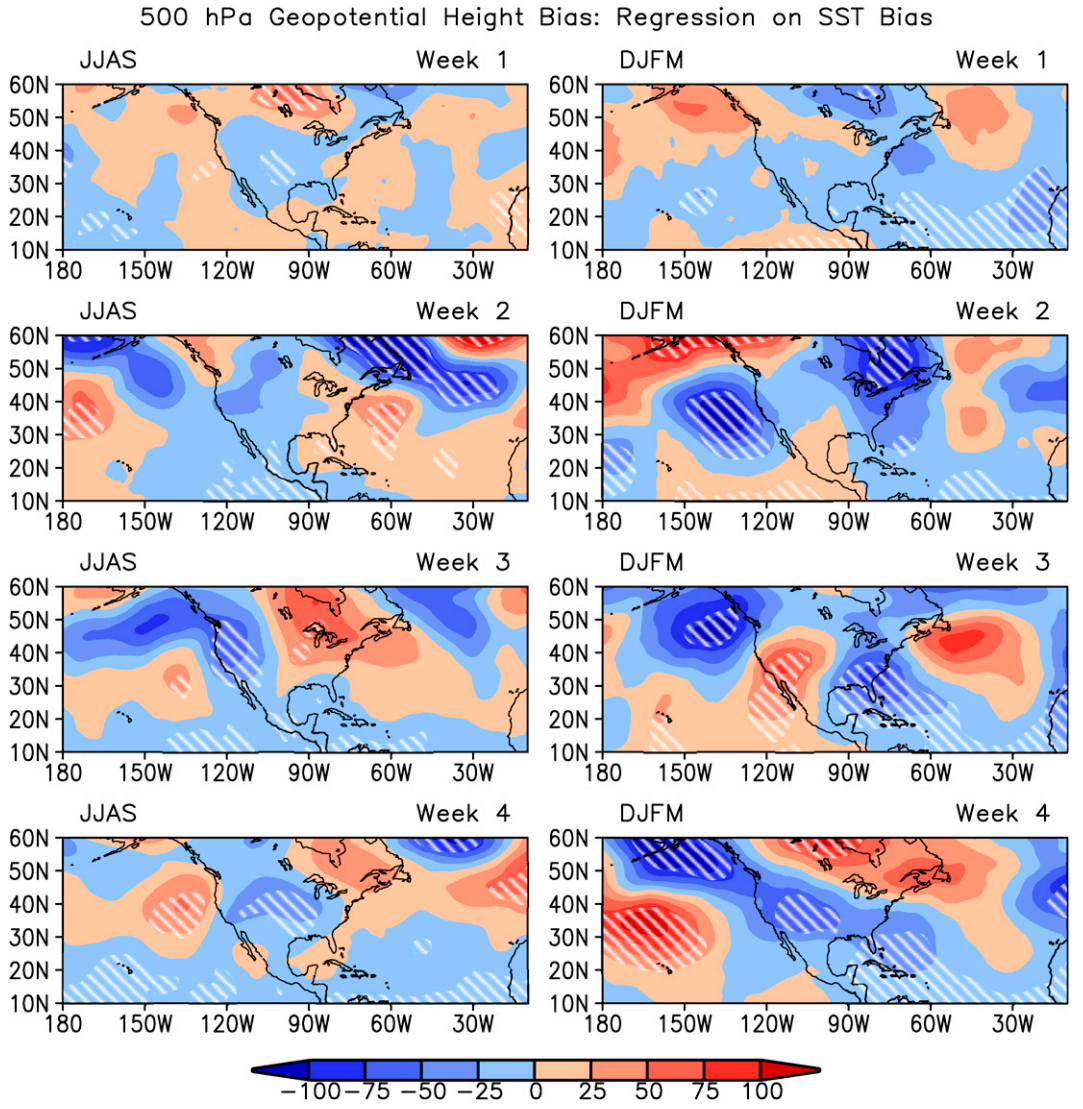

FIG. 6. Regression of bias (model forecast minus reanalysis) in the daily mean 500 hPa geopotential height on the equatorial index of the bias (model forecast minus observation) in the daily mean SST for the first 4 weeks of forecasts during (left) JJAS and (right) DJFM. The SST index is the area average over 10°S–10°N, 120°E–180°. The regions where the regression coefficient is statistically significant above 5% are hatched. Units are in gpm per unit standard deviation of the SST time series. The forecasts initiated from the first and fifteenth each month of JJAS and DJFM during 2011–18 are used in computing the regression.

The lag-0 regression maps of Z500 biases are shown in Fig. 6 for both boreal summer and winter. Most bias centers described in Figs. 2–5 are significantly related to the tropical SST bias. During boreal summer, in the first week of the forecast the Z500 bias on the order of 10 gpm noticed over most of the United States in Fig. 4 can be explained by a bias in the SST with the magnitude about one standard deviation. During week 2, the amplitude of regression coefficients increases slightly but the increase is not significant. During weeks 3 and 4 the regression pattern projects well onto the pattern of Z500 biases described in Fig. 4. The pattern of Z500 biases coherent with tropical SST biases closely resembles the Rossby wave train propagating northeastward from the tropics into the extratropics with negative biases in the tropical Pacific in conjunction with positive tropical SST biases and positive biases along the West Coast of the United States associated with negative tropical SST biases. Over the eastern half of the United States, positive biases are in conjunction with positive equatorial SST biases. During boreal winter, the regression pattern is similar to summer, but with larger values and significant areas. During week 3, the regression pattern resembles the Pacific–North American (PNA)-like atmospheric circulation pattern. PNA is the Northern Hemisphere extratropical response to El Niño–Southern Oscillation (ENSO; e.g., Lin and Derome 1999). The regression patterns are displaced slightly southward compared to the corresponding Z500 biases.

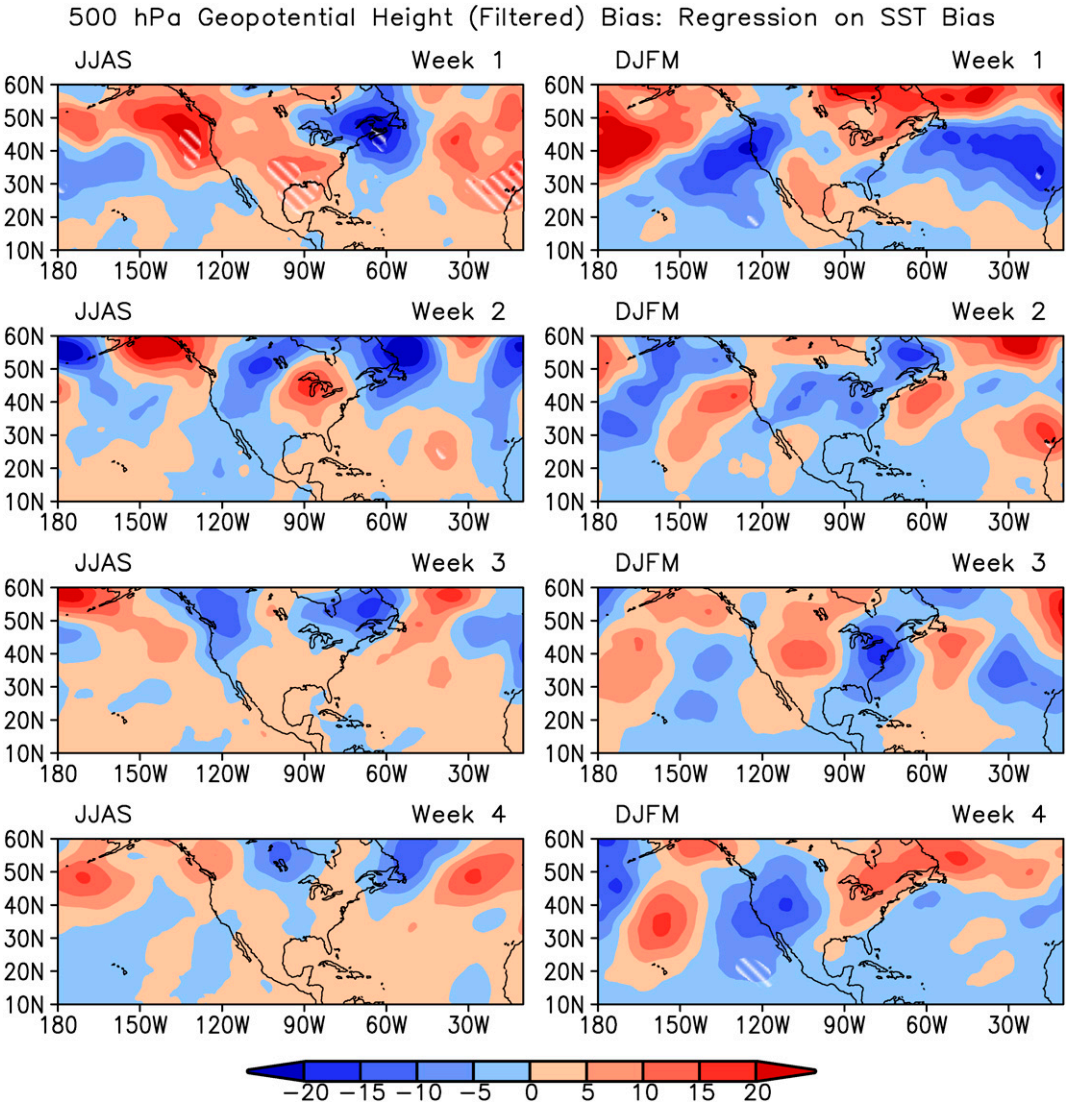

FIG. 7. Regression of bias (model forecast minus reanalysis) in the 8-day high-pass filtered daily anomaly of 500 hPa geopotential height on the equatorial index of the bias (model forecast minus observation) in the daily mean SST for the first 4 weeks of forecasts during (left) JJAS and (right) DJFM. The SST index is the area average over 10°S–10°N, 120°E–180°. The regions where the regression coefficient is statistically significant above 5% are hatched. Units are in gpm per unit standard deviation of the SST time series. The forecasts initiated from the first and fifteenth each month of JJAS and DJFM during 2011–18 are used in computing the regression.

A possible mechanism for this connection is that a warm bias in the equatorial Pacific can excite an anomalous heating over the region (Chang et al. 2006), which results in a Rossby wave train propagating northeastward.

The regression coefficients of bias in the 8-day high-pass filtered daily Z500 anomaly on the equatorial SST index are much weaker and not statistically significant (Fig. 7). This result suggests that biases in high-frequency variability of Z500 are not related to tropical Pacific SST biases. The anomalous transient-eddy activity due to the Rossby wave train induced by SST bias is not robust. This analysis does not rule out the impact of SST biases on the storm tracks, as shown by the regression of biases in ΔZ^2 onto the SST index (Fig. 8). During boreal summer, week 2 shows a robust influence of tropical SST biases onto the North Pacific storm track and during boreal winter, the relationship is robust in week 1.

The regression of precipitation bias on the tropical SST index (Fig. 9) shows a few regions of robust SST influence although these regions change from season to season and from week to week within the same season. In boreal summer, a small region over Nevada is statistically significant in week 1. Interestingly enough, the precipitation bias (Fig. 2) over this region has a different sign than the adjacent regions. The negative precipitation bias in this region may be the response to a negative SST bias.

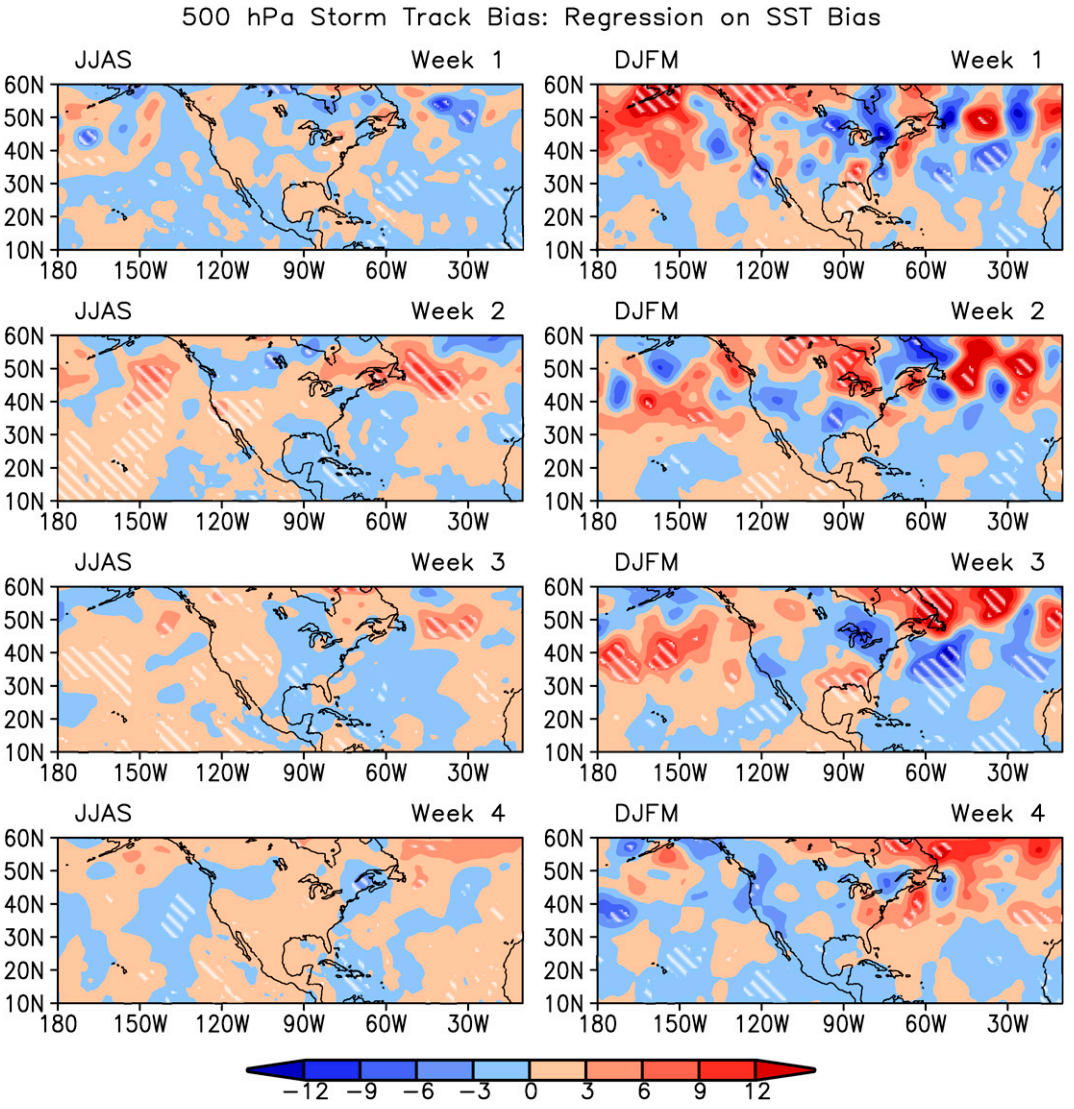

FIG. 8. Regression of bias (model forecast minus reanalysis) in the daily storm track based on ΔZ^2 [see Eq. (1) for definition and details] on the equatorial index of the bias (model forecast minus observation) in the daily mean SST for the first 4 weeks of forecasts during (left) JJAS and (right) DJFM. The SST index is the area average over 10°S–10°N, 120°E–180°. The regions where the regression coefficient is statistically significant above 5% are hatched. Units are in 0.001 gpm^2 per unit standard deviation of the SST time series. The forecasts initiated from the first and fifteenth each month of JJAS and DJFM during 2011–17 are used in computing the regression.

In week 2 this region expands over southwestern Oregon and remote northeastern California. However, the regression coefficients change sign. This region with significant regression is covered by a negative precipitation bias (Fig. 2) and may be the response to a negative SST bias. During the same week, another region with robust SST influence develops over the northern half of Georgia. The positive precipitation bias (Fig. 2) over this area suggests that it may be the response to a positive tropical SST bias. During week 3, the region in the northwestern United States continues to shift northward covering Oregon, Washington State, and a small fraction of central Idaho.

The region in the southeastern United States shifts southward over southern Georgia and Florida. Two more regions with robust SST influence develop during this week. The new regions have larger areal extent. The first region with positive values of regression covers most of the Four Corners. These regions are covered by coherent positive precipitation biases, suggesting they may be the response of positive SST biases.

The second region with large negative values of regression covers an extended area that spans across Arkansas, Missouri, Illinois, and Indiana. The precipitation biases (Fig. 2) over this area are mostly positive but also show some patches of negative biases suggesting a strong influence from local land–atmosphere

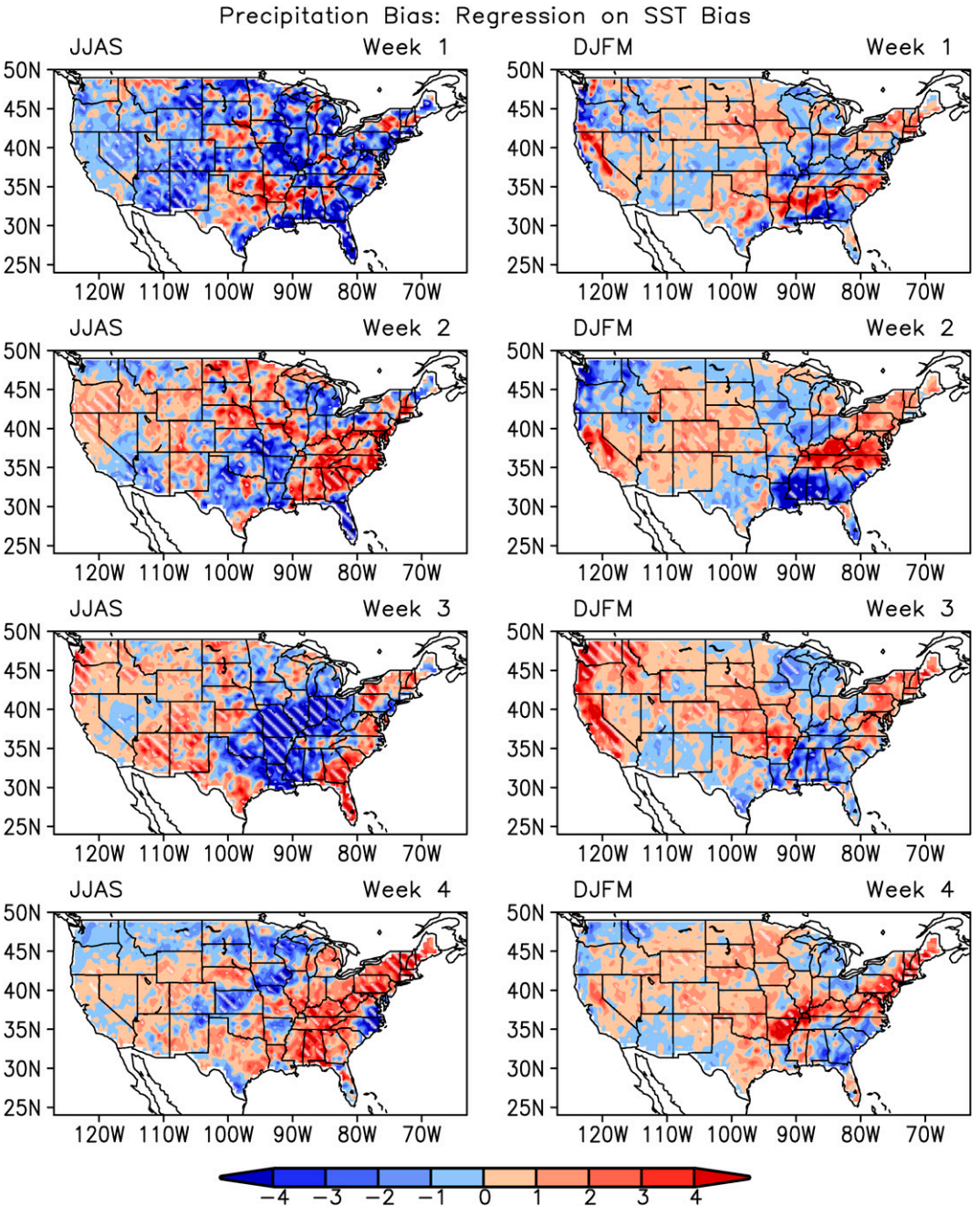

FIG. 9. Regression of bias (model forecast minus observation) in the daily mean precipitation on the equatorial index of the bias (model forecast minus observation) in the daily mean SST for the first 4 weeks of forecasts during (left) JJAS and (right) DJFM. The SST index is the area average over 10°S–10°N, 120°E–180°. The regions where the regression coefficient is statistically significant above 5% are hatched. Units are in mm day^{-1} per unit standard deviation of the SST time series. The forecasts initiated from the first and fifteenth each month of JJAS and DJFM during 2011–18 are used in computing the regression.

interaction effects. During week 4, the region with significant regression resembles the El Niño response along the East Coast of the United States.

In the case of surface temperature (Fig. 10), regions with significant values of the regression coefficients cover large areas especially during the summer. In boreal summer, the first 3 weeks are dominated by extensive regions with positive values of the regression coefficients. Over these regions, surface temperatures in the forecast have a warm bias (Fig. 3) suggesting a possible influence of the warm SST bias, but some notable

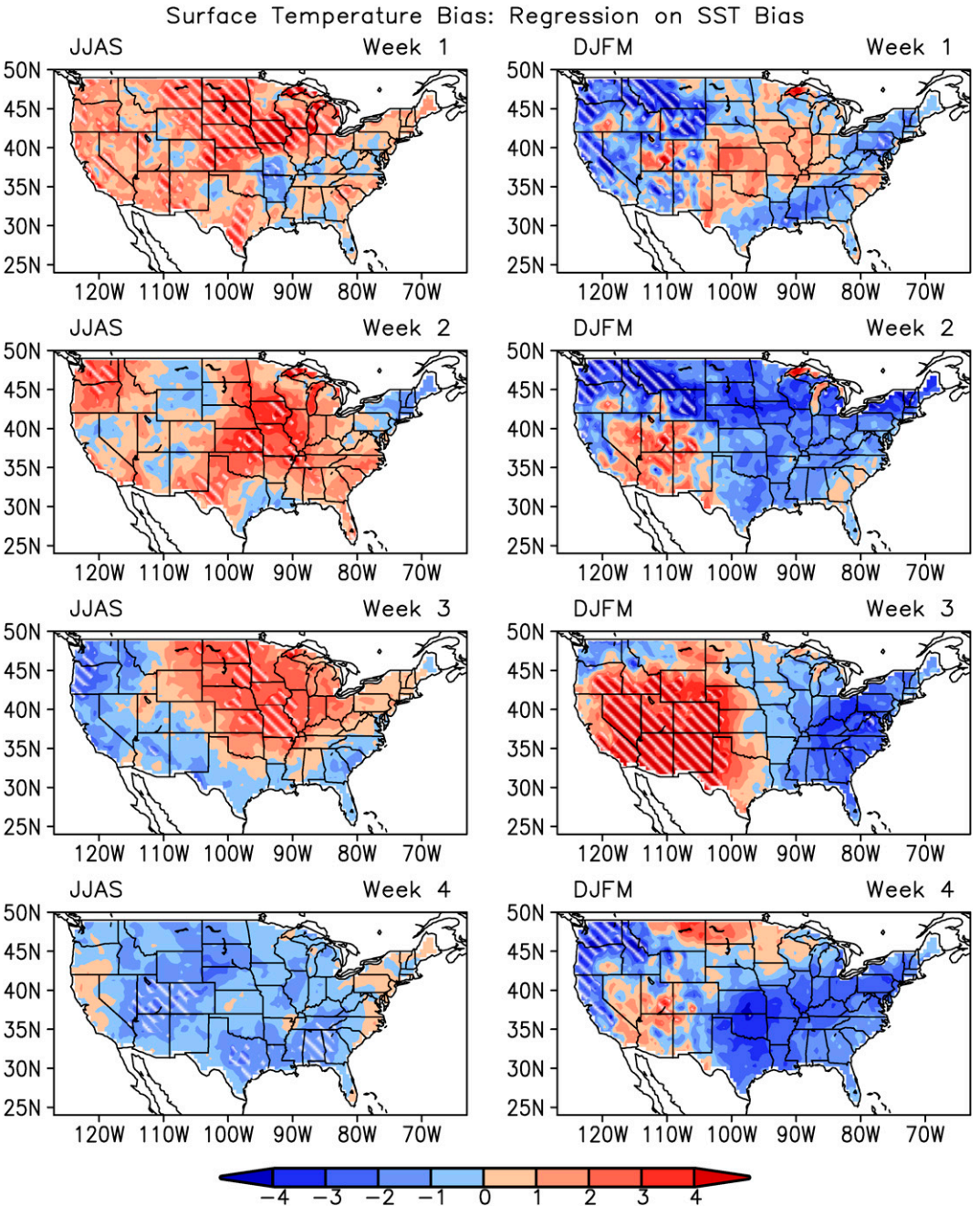

FIG. 10. Regression of bias (model forecast minus observation) in the daily mean surface temperature on the equatorial index of the bias (model forecast minus observation) in the daily mean SST for the first 4 weeks of forecasts during (left) JJAS and (right) DJFM. The SST index is the area average over 10°S–10°N, 120°E–180°. The regions where the regression coefficient is statistically significant above 5% are hatched. Units are in K per unit standard deviation of the SST time series. The forecasts initiated from the first and fifteenth each month of JJAS and DJFM during 2011–18 are used in computing the regression.

differences exist between the regression and bias patterns. The location of regions with robust regression is similar to the position of regions with maximum forecast errors in the warming trend signal of the surface air temperature documented by Krishnamurthy et al. (2021). A close correspondence can be seen between the regression and bias patterns along the West Coast of the United States, but with weak significance. The areas influenced by SST biases in weeks 2 and 3 are different than those in week 1. In week 4, the region in the southeastern United States with significant regression is affected by a cold

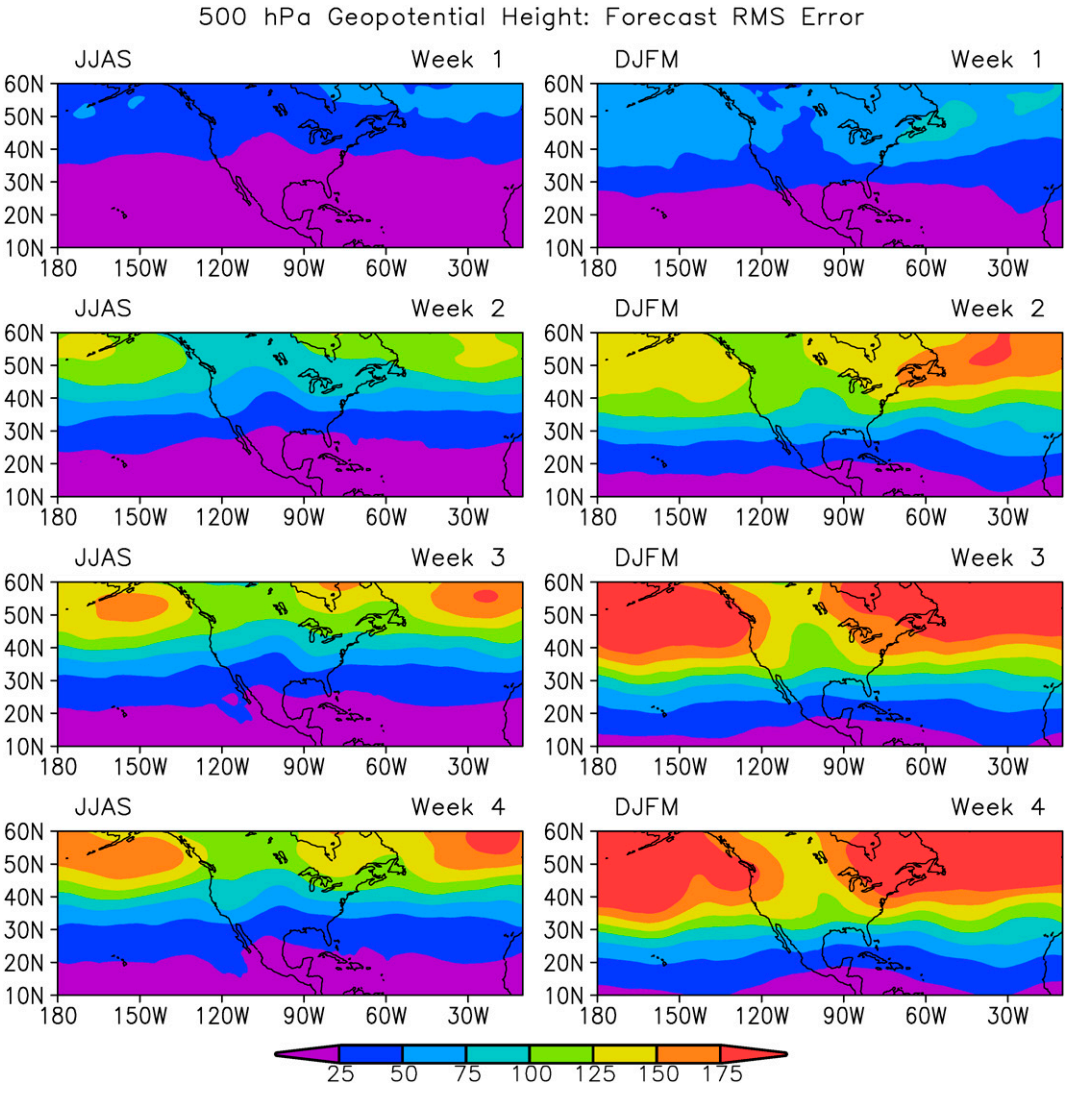

FIG. 11. RMS error in the forecasts of daily mean 500 hPa geopotential height (gpm) for the first 4 weeks of forecasts during (left) JJAS and (right) DJFM. The forecasts initiated from the first and fifteenth each month of JJAS and DJFM during 2011–18 are used in computing the RMS error.

bias (Fig. 5) suggesting a possible connection to the SST bias. The contrast between the regression patterns in the first 3 weeks and week 4 suggests the existence of SST biases in the initial conditions rather than biases developed as forecasts evolve. The most interesting result is seen during boreal winter, when the influence of SST bias is not significant with the exception of week 3, when a large area is covered by positive values of the regression coefficients. In this area, the forecast has a warm bias in the surface temperature, which is highly likely to be related to the tropical SST bias. Contrary to the expectation of an increase of the SST influence at longer time leads, in week 4 the region with strong regression changes sign and is not significant.

To determine the proportion of midlatitude biases (the dependent variable in our regression model) that can be explained by the tropical SST biases (independent variable), the R^2 coefficient is shown in Figs. S2–S5 (see the online supplemental material). The fraction explained by the tropical Pacific SST bias is ~6.25% for dynamical fields (geopotential height, temperature, and storm track) and ~5% for precipitation. Despite of relatively small values of R^2, regions with the largest values are also those with robust correlations.

The remaining fraction of biases not explained by the SST biases could be attributed to local effects, the global warming induced by the Indian Ocean warming (Schott et al. 2009) and tropical western Pacific (S.-P. Xie et al. 2010), as well as biases in the Atlantic Ocean (Johnson et al. 2020).

c. *Relationship between forecast biases and forecast errors*

Forecast biases result from the assumptions that numerical model makes about the predicted processes and numerical

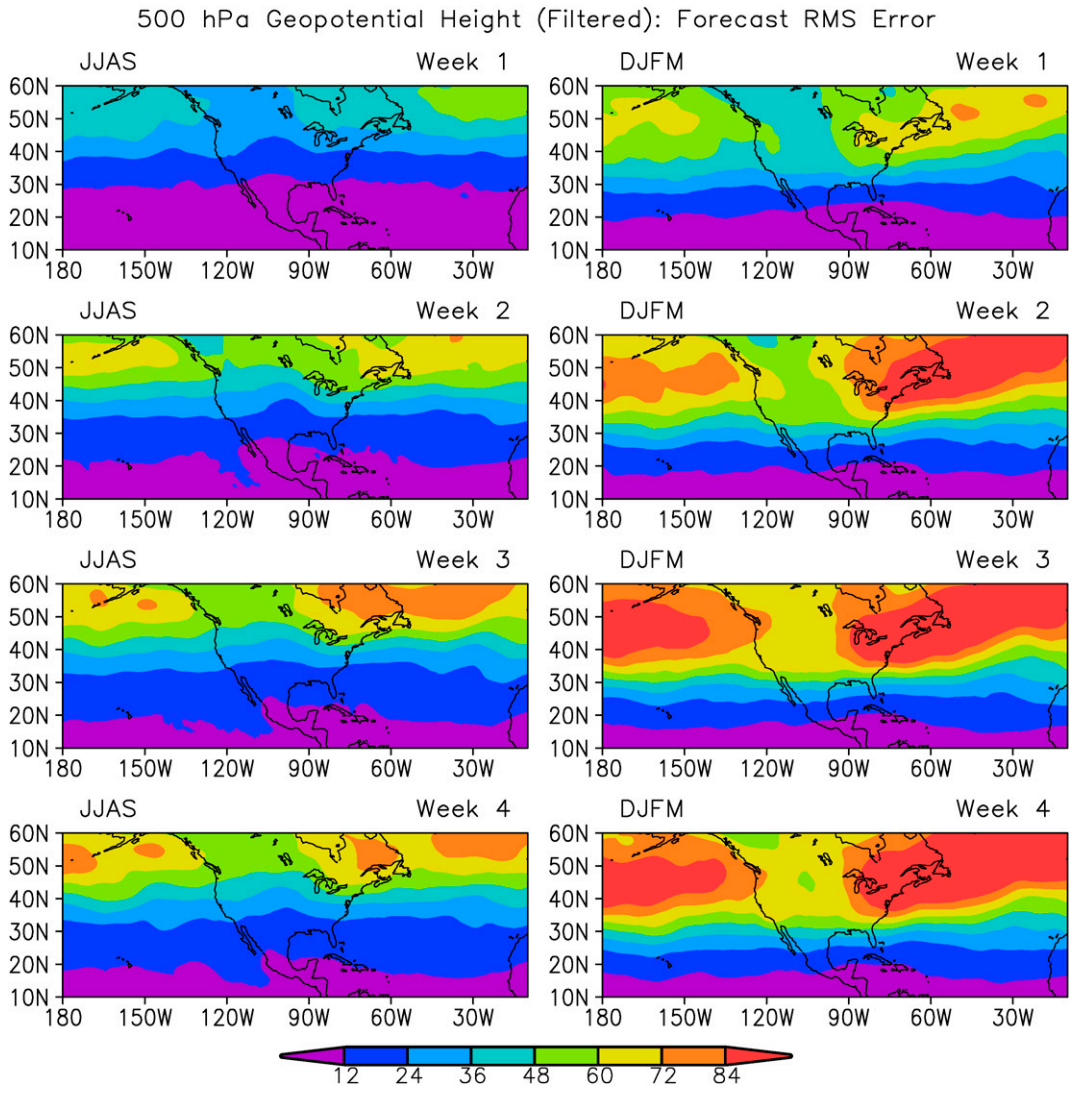

FIG. 12. RMS error in the forecasts of 8-day high-pass filtered daily anomaly of 500 hPa geopotential height (gpm) for the first 4 weeks of forecasts during (left) JJAS and (right) DJFM. The forecasts initiated from the first and fifteenth each month of JJAS and DJFM during 2011–18 are used in computing the RMS error.

schemes used for solving the model's equations. Forecast errors result from random variations in the system. Because forecast error has no preferred direction and magnitude, it can be reduced by averaging over a large number of forecasts. Conversely, bias has a net direction and magnitude. As a result, averaging over a large number of forecasts will not eliminate the effect of bias. The error is computed after the model calibration, a process in which model bias is removed.

To evaluate the relationship between the forecast biases induced by the tropical Pacific SST biases and forecast errors, Figs. 11–14 show the root-mean-square error (RMSE) of Z500 (raw and filtered values), precipitation, and surface temperature. A comparison of the RMSE to the regression maps (Figs. 6–10) suggests a qualitative relationship between the forecast errors and biases across all meteorological parameters analyzed. While regression coefficients have positive and negative values, the RMSE values are positively defined, meaning that a positive and a negative value of the regression coefficient can lead to the same forecast error. In these comparisons, a relationship between forecast errors and forecast biases over a region is assumed to occur if that region is dominated at the same time by large RMSE values and significant values of regression.

During boreal summer, the region in the central United States with significant Z500 biases shows changes in the unfiltered (Fig. 11) and filtered (Fig. 12) RMSEs in both upstream and downstream zonal directions. During boreal winter, starting from week 2 there is a good correspondence between the regions with significant unfiltered Z500 biases and large RMSEs.

A relationship between precipitation biases and forecast errors is not obvious during boreal summer (Fig. 13). During boreal winter, there is a good correspondence between

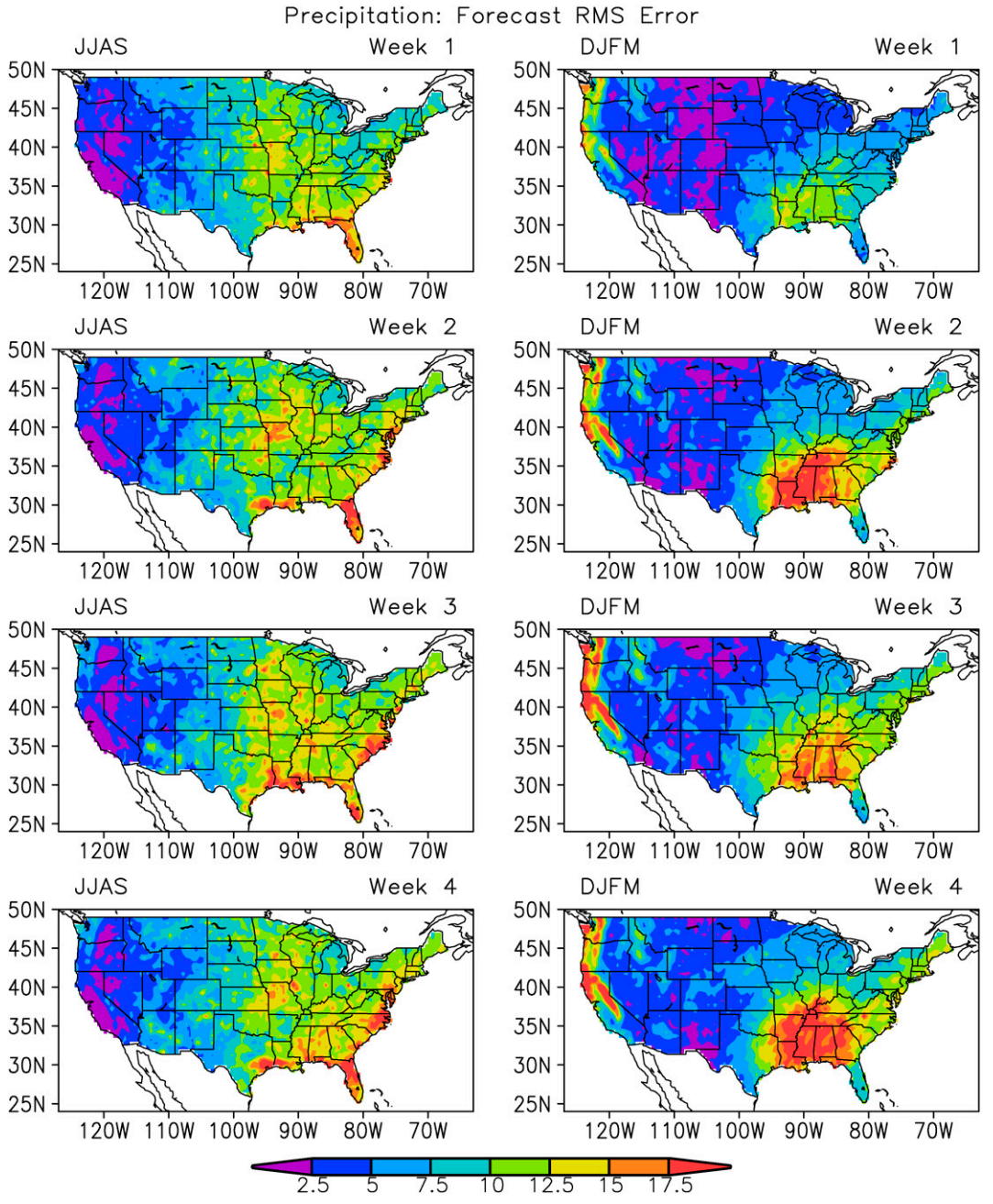

FIG. 13. RMS error in the forecasts of daily mean precipitation (mm day^{-1}) for the first 4 weeks of forecasts during (left) JJAS and (right) DJFM. The forecasts initiated from the first and fifteenth each month of JJAS and DJFM during 2011–18 are used in computing the RMS error.

the region with large RMSE in the southeastern United States (Fig. 13) and biases over this region (Fig. 9). However, the impact of SST biases over the southeastern United States is not robust.

Surface temperature (Fig. 14) displays the most obvious connections between the biases and forecast errors at all lead times during both seasons. In boreal summer, the region with large RMSEs that persist from week 1 though week 4 parallel to the West Coast of the United States corresponds to a region with significant influence from the tropical SST bias (Fig. 10). The RMSEs in the central United States can also be linked to the regression patterns over these regions. In boreal winter, during week 3 the large area with significant relationship between surface temperature biases and SST biases has some correspondence to the pattern of RMSEs, although in this area the forecast errors do not reach a maximum. In week 4

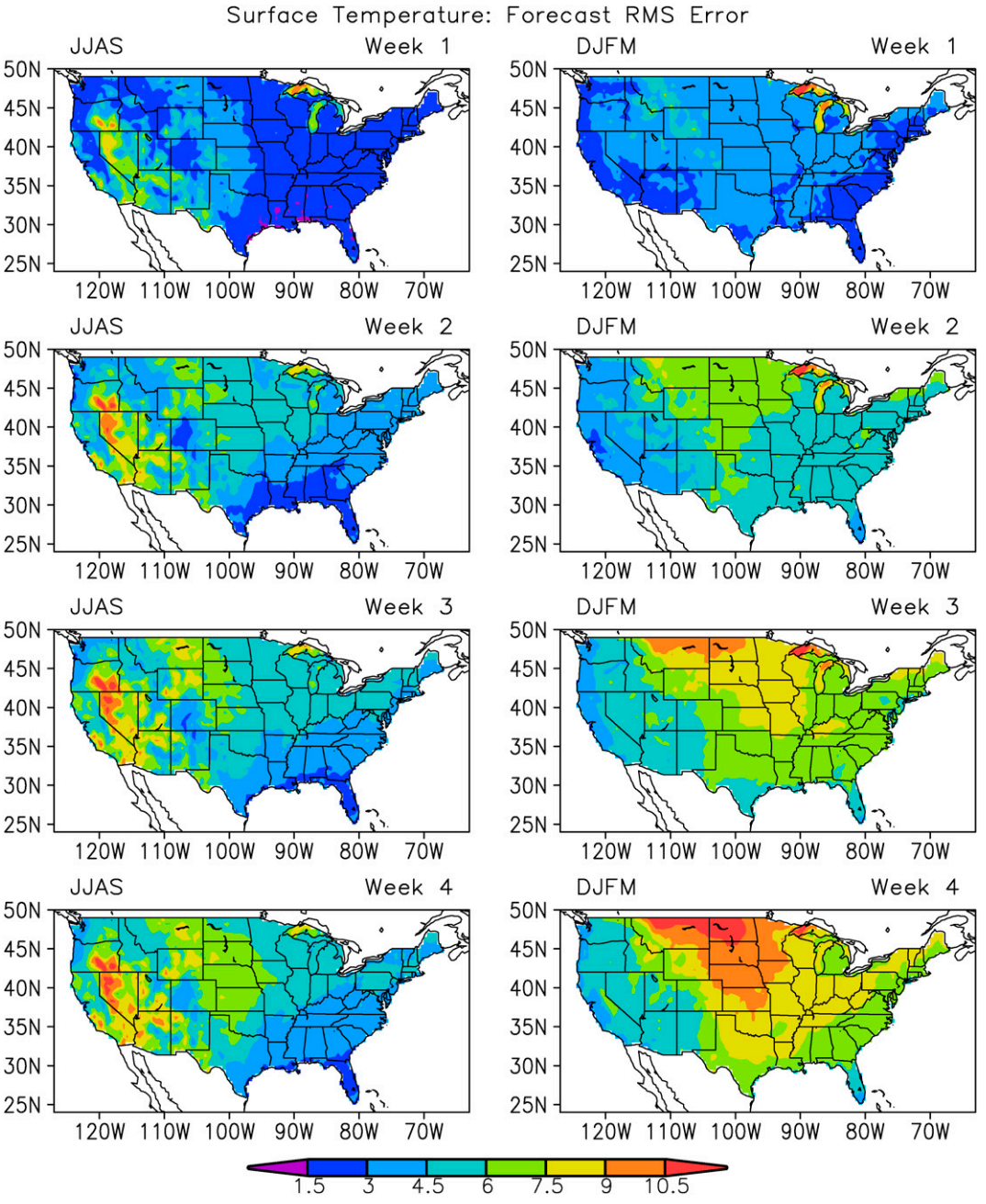

FIG. 14. RMS error in the forecasts of the daily mean surface temperature (K) for the first 4 weeks of forecasts during (left) JJAS and (right) DJFM. The forecasts initiated from the first and fifteenth each month of JJAS and DJFM during 2011–18 are used in computing the RMS error.

the region with maximum RMSEs has a correspondence to the regression map (Fig. 10); however, the regression pattern is not robust.

4. Discussion and conclusions

This study evaluated the biases that develop in the first 4 weeks of a set of deterministic forecasts produced with the coupled model UFS. Assuming that SST biases in the tropical Pacific can affect extratropical biases, the relationship between the SST biases in the deep tropics of the Pacific and surface and tropospheric weather was also investigated. The strength of the relationship was measured by the linear regression of an area average equatorial index and meteorological variables over the CONUS. Results of the regression analysis suggest a robust influence of the SST biases on the biases in the

large-scale circulation, surface precipitation, and temperature. The SST influence manifests at all lead times with an increasing influence from week 2 to week 4 for most fields with the exception of surface temperature, which also shows a strong influence of SST bias during the first week of the forecast.

The relationship between tropical SST bias and bias in the northern Pacific storm track has also been explored and results of the analysis indicated a weak linkage. The UFS model predicts a weaker than observed extratropical storm-track intensity; however, this bias is not related to the tropical SST bias. Similar to findings of Small et al. (2019), the bias in the storm-track strength is likely caused by the cold SST bias in the northwest Pacific. In some climate models, this cold bias is related to the horizontal resolution of the ocean model (Woollings et al. 2010; Small et al. 2019). Other studies indicate that midlatitude SST fronts associated with the Kuroshio affect the variability of storm track (Nakamura et al. 2008).

A qualitative relationship between the SST-induced biases and forecast errors measured by the RMSE has been explored. The comparison between regression and RMSE showed large areas of agreements. Thus, the RMSE of the forecast can be minimized by removing the bias in the meteorological field that is related to the tropical SST bias.

This study is limited to the influence of tropical Pacific SST bias onto the atmospheric variability over CONUS. Vitart and Balmaseda (2018) showed that in the ECMWF model, week 4 precipitation biases over CONUS have a small influence from SST biases in the Atlantic Ocean. These influences of SST biases will be addressed in a future study.

Acknowledgments. C. Stan, V. Krishnamurthy, and H. Bai were supported by the National Oceanic and Atmospheric Administration (Grant NA18NWS4680069) and by the Unified Forecast System Research to Operation (UFS R2O) project which is jointly funded by NOAA's Office of Science and Technology Integration (OSTI) of National Weather Service (NWS) and Weather Program Office (WPO) [Joint Technology Transfer Initiative (JTTI)] of the Office of Oceanic and Atmospheric Research (OAR) through the NOAA Grant NA19NES4320002 [Cooperative Institute for Satellite Earth System Studies (CISESS)].

Data availability statement. UFS data used in this study are publicly available at https://registry.opendata.aws/noaa-ufs-s2s/. ERAI data can be downloaded from https://www.ecmwf.int/en/forecasts/datasetsreanalysis-datasets/era-interim. CPC Global Unified Precipitation and Temperature, and OISST2 data provided by the NOAA/OAR/ESRL/PSL, Boulder, Colorado, can be downloaded from their website at https://psl.noaa.gov/data/gridded/.

REFERENCES

Adcroft, A. W., and Coauthors, 2019: The GFDL global ocean and sea ice model OM4.0: Model description and simulation features. *J. Adv. Model. Earth Syst.*, **11**, 3167–3211, https://doi.org/10.1029/2019MS001726.

Balaguru, K., L. P. van Roekel, L. R. Leung, and M. Veneziani, 2021: Subtropical eastern North Pacific SST bias in Earth system models. *J. Geophys. Res. Oceans*, **126**, e2021JC017359, https://doi.org/10.1029/2021JC017359.

Bretherton, C. S., M. Widmann, V. P. Dymnikov, J. M. Wallace, and I. Blade, 1999: The effective number of spatial degrees of freedom of a time-varying field. *J. Climate*, **12**, 1990–2009, https://doi.org/10.1175/1520-0442(1999)012<1990:TENOSD>2.0.CO;2.

Chang, P. T., and Coauthors, 2006: Climate fluctuations of tropical coupled systems—The role of ocean dynamics. *J. Climate*, **19**, 5122–5174, https://doi.org/10.1175/JCLI3903.1.

Cook, B. I., A. P. Williams, J. S. Mankin, R. Seager, J. E. Smerdon, and D. Singh, 2018: Revisiting the leading drivers of Pacific coastal drought variability in the contiguous United States. *J. Climate*, **31**, 25–43, https://doi.org/10.1175/JCLI-D-17-0172.1.

Dee, D. P., and Coauthors, 2011: The ERA-Interim reanalysis: Configuration and performance of the data assimilation system. *Quart. J. Roy. Meteor. Soc.*, **137**, 553–597, https://doi.org/10.1002/qj.828.

Emery, W. J., 2015: Sea surface temperature. *Encyclopedia of Atmospheric Sciences*, Cambridge University Press, 136–143.

Hamming, R. W., 1989: *Digital Filters*. 3rd ed. Prentice Hall, 284 pp.

Harris, L. M., and S.-J. Lin, 2013: A two way nested global-regional dynamical core on the cubed-sphere grid. *Mon. Wea. Rev.*, **141**, 283–306, https://doi.org/10.1175/MWR-D-11-00201.1.

Hu, Z.-Z., B. Huang, Y.-T. Hou, W. Wang, F. Yang, C. Stan, and E. K. Schneider, 2011: Sensitivity of tropical climate to low-level clouds in the NCEP Climate Forecast System. *Climate Dyn.*, **36**, 1795–1811, https://doi.org/10.1007/s00382-010-0797-z.

Johnson, N. C., D. C. Collins, S. B. Feldstein, M. L. L'Heureux, and E. E. Riddle, 2014: Skillful wintertime North American temperature forecast out to 4 weeks based on the state of ENSO and the MJO. *Wea. Forecasting*, **29**, 23–38, https://doi.org/10.1175/WAF-D-13-00102.1.

——, L. Krishnamurthy, A. T. Wittenberg, B. Xiang, G. A. Vecchi, S. B. Kapnick, and S. Pascale, 2020: The impact of sea surface temperature biases on North American precipitation in a high-resolution climate model. *J. Climate*, **33**, 2427–2447, https://doi.org/10.1175/JCLI-D-19-0417.1.

Krishnamurthy, V., and C. Stan, 2022: Prediction of extreme events in precipitation and temperature over CONUS during boreal summer in the UFS coupled model. *Climate Dyn.*, **59**, 109–125, https://doi.org/10.1007/s00382-021-06120-0.

——, and Coauthors, 2021: Sources of subseasonal predictability over CONUS during boreal summer. *J. Climate*, **34**, 3273–3294, https://doi.org/10.1175/JCLI-D-20-0586.1.

Li, G., and S.-P. Xie, 2014: Tropical biases in CMIP5 multi-model ensemble: The excessive equatorial Pacific cold tongue and double ITCZ problems. *J. Climate*, **27**, 1765–1780, https://doi.org/10.1175/JCLI-D-13-00337.1.

Lin, H., and J. Derome, 1999: The genesis and predictability of persistent Pacific–North American anomalies in a model atmosphere. *Tellus*, **51A**, 686–697, https://doi.org/10.3402/tellusa.v51i5.14487.

Murphy, A. H., 1993: What is a good forecast? An essay on the nature of goodness in weather forecasting. *Wea. Forecasting*, **8**, 281–293, https://doi.org/10.1175/1520-0434(1993)008<0281:WIAGFA>2.0.CO;2.

Nakamura, H., T. Sampe, A. Goto, W. Ohfuchi, and S.-P. Xie, 2008: On the importance of midlatitude oceanic frontal zones for the mean state and dominant variability in the

tropospheric circulation. *Geophys. Res. Lett.*, **35**, L15709, https://doi.org/10.1029/2008GL034010.

Putman, W. M., and S.-J. Lin, 2007: Finite-volume transport on various cubed-sphere grids. *J. Comput. Phys.*, **227**, 55–78, https://doi.org/10.1016/j.jcp.2007.07.022.

Reynolds, R. W., T. M. Smith, C. Liu, D. B. Chelton, K. S. Casey, and M. G. Schlax, 2007: Daily high-resolution-blended analyses for sea surface temperature. *J. Climate*, **20**, 5473–5496, https://doi.org/10.1175/2007JCLI1824.1.

Saha, S., and Coauthors, 2014: The NCEP Climate Forecast System version 2. *J. Climate*, **27**, 2185–2208, https://doi.org/10.1175/JCLI-D-12-00823.1.

Schott, F. A., S.-P. Xie, and J. P. McCreary, 2009: Indian Ocean circulation and climate variability. *Rev. Geophys.*, **47**, RG1002, https://doi.org/10.1029/2007RG000245.

Small, R. J., R. Msadek, Y.-O. Kwon, J. F. Booth, and C. Zarzycki, 2019: Atmosphere surface storm track response to resolved ocean mesoscale in two sets of global climate model experiments. *Climate Dyn.*, **52**, 2067–2089, https://doi.org/10.1007/s00382-018-4237-9.

Stan, C., and B. P. Kirtman, 2008: The influence of atmospheric noise and uncertainty in ocean initial conditions on the limit of predictability of a coupled GCM. *J. Climate*, **21**, 3487–3503, https://doi.org/10.1175/2007JCLI2071.1.

——, M. Khairoutdinov, C. A. DeMott, V. Krishnamurthy, D. M. Straus, D. A. Randall, J. L. Kinter III, and J. Shukla, 2010: An ocean-atmosphere climate simulation with an embedded cloud resolving model. *Geophys. Res. Lett.*, **37**, L01702, https://doi.org/10.1029/2009GL040822.

Stefanova, L., and Coauthors, 2022: Description and results from UFS coupled prototypes for future global, ensemble and seasonal forecasts at NCEP. NCEP Office Note 510, 201 pp., https://doi.org/10.25923/knxm-kz26.

Vellinga, M., D. Copsey, T. Graham, S. Milton, and T. Johns, 2020: Evaluating benefits of two-way ocean–atmosphere coupling for global NWP forecasts. *Wea. Forecasting*, **35**, 2127–2144, https://doi.org/10.1175/WAF-D-20-0035.1.

Vitart, F., and M. Balmaseda, 2018: Impact of sea surface temperature biases on extended-range forecasts. ECMWF Tech. Memo. 830, 19 pp., https://www.ecmwf.int/node/18659.

——, and Coauthors, 2017: The Subseasonal to Seasonal (S2S) Prediction project database. *Bull. Amer. Meteor. Soc.*, **98**, 163–173, https://doi.org/10.1175/BAMS-D-16-0017.1.

Woollings, T. B., B. Hoskins, M. Blackburn, D. Hassell, and K. Hodges, 2010: Storm track sensitivity to sea surface temperature resolution in a regional atmosphere model. *Climate Dyn.*, **35**, 341–353, https://doi.org/10.1007/s00382-009-0554-3.

WW3DG, 2019: User manual and system documentation of WAVEWATCH III version 6.07. NOAA/NWS/NCEP/MMAB Tech. Note 333, 465 pp., https://github.com/NOAA-EMC/WW3/wiki/Manual.

Xie, P., M. Chen, and W. Shi, 2010: CPC unified gauge-based analysis of global daily precipitation. *24th Conf. on Hydrology*, Atlanta, GA, Amer. Meteor. Soc., 2.3A, https://ams.confex.com/ams/90annual/techprogram/paper_163676.htm.

Xie, S.-P., C. Deser, G. A. Vecchi, J. Ma, H. Teng, and A. Witterberg, 2010: Global warming pattern formation: Sea surface temperature and rainfall. *J. Climate*, **23**, 966–986, https://doi.org/10.1175/2009JCLI3329.1.

Yau, A. M.-W., and E. K.-M. Chang, 2020: Finding storm track activity metrics that are highly correlated with weather impacts. Part I: Frameworks for evaluation and accumulated track activity. *J. Climate*, **33**, 10 169–10 186, https://doi.org/10.1175/JCLI-D-20-0393.1.

Zuidema, P. P., and Coauthors, 2016: Challenges and prospects for reducing coupled climate model SST biases in the eastern tropical Atlantic and Pacific Oceans: The U.S. CLIVAR Eastern Tropical Oceans Synthesis Working Group. *Bull. Amer. Meteor. Soc.*, **97**, 2305–2328, https://doi.org/10.1175/BAMS-D-15-00274.1.